CONF-8704177--7

ANL-HEP-CP-87-62

HADRON PRODUCTION IN e^+e^- ANNIHILATION AT 29 GeV*†

(Recent results from HRS)

K. Sugano
Argonne National Laboratory
Argonne, IL 60439

ANL-HEP-CP--87-62

DE88 003110

Abstract

Recent results from HRS on the production of scalar, tensor, and charm mesons and of strange and charm baryons in e^+e^- annihilation are presented. The production of $f_0(975)$, $f_2(1270)$, and $K_2^*(1430)$ is shown briefly. The decays of $D^*(2010)^+$ and $D^*(2007)^0$ are studied in detail. The production of Ξ^- and $\Sigma(1385)^\pm$ is mentioned. Finally, the preliminary analyses of Λ_c and $\Sigma_c^{0,++}$ productions are presented.

1. Introduction

In e^+e^- annihilation at 29 GeV, various kinds of particles are produced through the cascade of primary quarks; e^+e^- goes into $q\bar{q}$ and subsequently these quarks become hadrons. Since the primary quarks are produced according to the square of their electric charges, we expect a copious production of light particles and charm particles. Besides this mechanism, there are radiations of hard gluons which are expected to hadronize into particles somewhat differently from quarks. Diquarks are also created during the hadronization process resulting in various baryons. There may be a chance that some exotic particles such as glueballs, hybrids, and four-quark states are produced.

Because of the simplicity of e^+e^- annihilation, there are two finely-tuned models which explain the hadronization mechanisms; one is the cluster fragmentation model and the other the string fragmentation model. However, I will skip the details due to a time limitation.

From an experimental point of view, e^+e^- collision has many advantages in studying the production of hadrons. Some of them are a clean environment,

---

*An invited talk given at the Second International Conference on Hadron Spectroscopy (HADRON '87), KEK, Japan (April 16-18, 1987).

†Work supported in part by the U.S. Department of Energy, Division of High Energy Physics, under Contract W-31-109-ENG-38.

DISCLAIMER

almost 4π coverage, and a relatively general trigger. However, the disadvantages are low event rate due to a limited luminosity and relatively poor resolution for high momentum tracks. The data sample, upon which the physics results are based, corresponds to an integrated luminosity of 300 pb^{-1} obtained during the five years of operation of the High Resolution Spectrometer (HRS) at the PEP e^+e^- storage ring at a center of mass energy of 29 GeV.

The HRS detector is a solenoidal spectrometer that measures charged particles and electromagnetic energy over 90% of the solid angle as shown in Fig. 1. The details of the detector are given elsewhere.[1] Substantial emphasis is placed on measurements of the charged particle momenta and all the detector elements operate in a magnetic field of 1.62 T. The tracking system consists of a vertex chamber, a central drift chamber, and an outer drift chamber. The central drift chamber has 15 cylindrical layers of drift cells. Eight of the layers have stereo wires (±60 mrad) in order to measure the z position. The beam pipe and the inner wall of the central drift chamber are made of beryllium so as to minimize the multiple Coulomb scattering; the total material between the interaction point and the central drift chamber is less than 0.02 radiation length. The measured momentum resolution at large angle with respect to the beam is $\sigma_p/p \simeq 2 \times 10^{-3} p$ (p in GeV/c). The barrel calorimeter system for electromagnetic showers consists of a $3X_o$ Pb-scintillator sandwich, a single-layer of wire proportional chambers (PWC) in which the wires are aligned along the e^+e^- beam direction, and an $8X_o$ Pb-scintillator sandwich. The PWC plane is at a radius of 2.03 m from the interaction point. Each of the two scintillator sections is read out by two phototubes, one at each end of the approximately 3 m long modules. The energy resolution is $(\sigma_E/E)^2 = 0.16^2/E + 0.06^2$ (E in GeV). The positions of the electromagnetic showers along the beam direction, z, are measured by current division in the PWC wires to an accuracy of ~ 2.5 cm.

The apparatus was triggered when two more tracks were found by the trigger processor in the central drift chamber or when at least 4.8 GeV of energy was deposited in the barrel and endcap calorimeters. Subsequently, to select one-photon annihilation events and to reduce beam-gas and two-photon backgrounds, the events were required to have a minimum charged multiplicity of 5 and a scalar sum of charged track momenta greater than 10 GeV/c.

2. D^* Decays

We report a study of the decay widths of $D^*(2010)^+$ and $D^*(2007)^o$, the radiative decay branching ratio of D^{*o}, and the fragmentation function of D^{*o}. First the present upper limits of the D^* widths are $\Gamma_{D^{*+}} < 2.0$ MeV/c

and $\Gamma_{D^{*o}} < 5$ MeV/c^2. These widths are very narrow compared to the other light mesons despite the fact that the D^*'s decay strongly. There are indications that the D^* is one of the narrowest particles among the strongly decaying particles.[2] Therefore, it is worthwhile to improve the present upper limits in order to study the decay mechanisms.

The D^{*+} was reconstructed in the decay mode $D^{*+} \to D^o\pi^+ \to K^-\pi^+\pi^+$. Our analyses also include the charge conjugate states. For the $D^o \to K^-\pi^+$ decay mode, all the tracks coming from the vertex were tried in turn as both K and π. The cuts of $Z_D > 0.5$ and $|\cos\theta^*| < 0.7$ were applied, where $Z_D \equiv 2E_D/\sqrt{s}$ and θ^* is the D^o decay angle in the helicity frame. (D^o rest frame with the z axis along the D^o direction of flight.) The cos θ^* selection eliminates an angular region observed to be dominated by the background. The resulting invariant mass spectrum is shown in Fig. 2. A clear signal is observed at the D^o mass. The D^o signal was fitted with a polynomial form for the background and a Gaussian form for the signal. The fitted mass of (1861 ± 4)MeV/c^2 is consistent with the currently accepted value. The standard deviation (σ_m) of (13 ± 2) MeV/c^2 is consistent with the apparatus resolution as determined by a Monte Carlo simulation.

The D^* signal was reconstructed utilizing the fact that the Q value of the reaction is 5.8 MeV and the D^{*+}-D^o mass difference can therefore be determined extremely well. Figure 3 shows the distribution in the mass difference ($\Delta \equiv M_{K^-\pi^+\pi^+} - M_{K^-\pi^+}$) for $Z_{D^*} > 0.4$ with the D^o selection 1810 MeV/c^2 < $M_{K^-\pi^+}$ < 1920 MeV/c^2, which is the mass region for the D^o determined above. The peak in the distribution shows a clear signal for the D^{*+} production with small background. The distribution was fitted by polynomial background plus Gaussian signal. The resulting values are Δ = (145.34 ± 0.05) MeV/c^2 for the peak value and σ_Δ = (0.50 ± 0.05) MeV/c^2 for the standard deviation, where the errors are statistical only. The value of σ_Δ corresponds to the width Γ_Δ = (1.17 ± 0.06) MeV/c^2 as FWHM assuming a Gaussian form. The width remains the same within the statistical errors when the Z_{D^*} cut is changed from 0.4 up to 0.7. The background becomes less as the cut gets higher.

According to the Monte Carlo simulation of our detector, the apparatus resolution (standard deviation) of Δ is σ_Δ^{MC} = (0.33 ± 0.07 ± 0.07) MeV/c^2, where the first error is statistical and the second systematic. This corresponds to to the width of Γ_Δ^{MC} = (0.78 ± 0.16 ± 0.16) MeV/c^2. The observed width is consistent with the apparatus resolution within the errors, although the Monte Carlo value is 0.4 MeV/c^2 smaller than the observed one. The observed width of the mass difference is dominated by the detector resolution. Therefore, we put an upper limit of the directly measured D^{*+}

decay width as $\Gamma_{D^{*+}} < 1.26$ MeV/c^2 at 90% CL.

This direct measurement can be compared to a calculation based on the measured branching ratio of the D^{*+} radiative decay. Since the radiative decay $D^{*+} \to D^+\gamma$ is an M1 transition, the electromagnetic width is given by the following formula:

$$\Gamma_{M1} = \frac{4}{3}\alpha\left(\frac{e_c}{2m_c} + \frac{e_d}{2m_d}\right)^2 k^3 \qquad (1)$$

where $e_q/2m_q$ is the magnetic moment of the quark q (charm quark and down quark) and k is a momentum of photon. Therefore, the total decay width is given by $\Gamma_{D^{*+}} = \Gamma_{M1}/Br(D^{*+} \to D^+\gamma)$. The estimated value of Γ_{M1} for $D^{*+} \to D^+\gamma$ is about 1.1 keV/c^2, using the constituent quark masses ($m_c = 1.84$ GeV/c^2 and $m_d = 0.34$ GeV/c^2). The most recent measurement of the radiative decay mode is $Br(D^{*+} \to D^+\gamma) = (17 \pm 11)\%$.[3] This corresponds to the total width $\Gamma = 7 \pm {}^{12}_{3}$ keV/c^2, or $\Gamma < 22$ keV/c^2 at 90% CL, consistent with our result. Since there is some ambiguity in calculating the value of (1), our direct measurement is orthogonal to this approach.

There are also calculations of the hadronic decay widths of $D^{*+} \to D^+\pi^o$ and $D^{*+} \to D^o\pi^+$, based on the SU(4)-invariant interaction.[4] Using these calculations and the measured branching ratios of these processes, the total width of D^{*+} is (27 ± 5) keV/c^2. This value is higher than that calculated from the radiative decay mode. We need more accurate measurements of the radiative decay.[5]

We used a different method to obtain an upper limit on the D^{*o} decay width. The $D^+\pi^-$ threshold is only 1.8 MeV above the mass of $D^*(2007)^o$. Therefore, if the width of D^{*o} is large enough, the decay mode of $D^{*o} \to D^+\pi^-$ will occur with a significant rate from the higher mass tail of the resonance.[6] Such examples are $f_0(975) \to K\bar{K}$ and $a_0(980) \to K\bar{K}$. Since there are indications that the D^{*o} has very narrow width, the branching ratio $D^{*o} \to D^+\pi^-$ through this mechanism is expected to be small. Consequently, even a moderate upper limit on this decay mode can result in a significant improvement in constraining the width of D^{*o} which is not yet well measured.

In reconstructing the D^+ through the $K^-\pi^+\pi^+$ decay mode, all the tracks coming from the vertex were tried in turn as both K and π. The cuts of $Z_D > 0.2$ and $|\cos\theta^*| > 0.3$ were applied. The resulting invariant mass spectrum with a more stringent cut of $Z_D > 0.6$ is shown in Fig. 4. A clear signal is observed at the D^+ mass. The D^+ signal was fitted with a polynomial form for the background and a Gaussian form for the signal. The fitted mass (1863 ± 4)

MeV/c^2 is consistent with the currently accepted value. The standard deviation (σ_m) of (17 ± 2) MeV/c^2 is consistent with with the apparatus resolution as determined by a Monte Carlo simulation.

The D^{*o} signal was searched in the mass difference distribution ($\Delta \equiv M_{K^-\pi^+\pi^+\pi^-} - M_{K^-\pi^+\pi^+}$) for $Z_{D^*} > 0.2$ with the D^+ selection 1820 MeV/c^2 < $M_{K^-\pi^+\pi^+}$ < 1900 MeV/c^2 which is the mass region for the D^+ determined above. This mass difference method gives better signal resolution and lower background than the direct reconstruction of $K^-\pi^+\pi^+\pi^+$ invariant mass. Figure 5 shows the mass difference distribution for the D^{*o}. The background was estimated by two methods. Firstly, the D^+ candidates from the side bands of the peak in Fig. 4 (1.6 GeV/c^2 < $M_{K^-\pi^+\pi^+}$ < 1.8 GeV/c^2 and 1.92 GeV/c^2 < $M_{K^-\pi^+\pi^+}$ < 2.12 GeV/c^2) were combined with the other π^-. Secondly, wrong sign combinations of $K^-\pi^+\pi^+\pi^+$ and $K^-\pi^+\pi^-\pi^+$ were studied. Both of these techniques gave a consistent shape within the statistical errors. The background data, fitted to a polynomial and normalized to the data in the region of 143 MeV/c^2 < Δ < 146 MeV/c^2 in the mass difference distribution, is shown as the solid curve in Fig. 5.

After subtracting the background, the resulting signal is 3 ± 15 events in the region of 137 MeV/c^2 < Δ < 143 MeV/c^2, which is consistent with no signal. The error comes mainly from the uncertainty in determining the background. This corresponds to an upper limit of the branching ratio as $B_r(D^{*o} \to D^+\pi^-)$ < 15% at 90% CL, assuming that the D^{*o} and D^{*+} production cross sections are equal. The detector acceptance is calculated from a Monte Carlo simulation. This upper limit of branching ratio gives upper limit on the width of $\Gamma_{D^{*o}}$ < 1.5 MeV/c^2 at 90% CL, assuming a p-wave Breit-Wigner form and a D^{*o} mass of 2007.2 MeV/c^2. This is a substantial improvement of the existing upper limit which is 5 MeV/c^2. Our limit can be further improved by a more accurate measurement of the D^{*o} mass.

We also studied the production cross sections and the radiative decay branching ratio of D^{*o}.[7] The D^{*o} was reconstructed in the decay mode $D^{*o} \to D^o\gamma \to K^-\pi^+\gamma$. A photon was defined as an isolated shower in the barrel calcrimeter with no associated charged particles. The position of a shower was determined using information from the proportional wire tubes. Three categories of photon were used: a single isolated photon in a shower counter module; one photon sharing a shower counter module with a second photon (in this case the energy deposited in this module was divided equally between the two photons); and one photon and one charged particle sharing a shower counter module (in this case the average energy deposited by a minimum-ionizing particle, which is 0.2 GeV, was subtracted from the total energy deposited in the module to determine the energy of the photon). Since the

angle between the D^0 direction and the photon in the lab frame, α, tends to be small, candidates corresponding to the $D^{*0} \to D^0\gamma$ decay were required to have $\cos\alpha > 0.9$ and further, the energy of the photon was required to be greater than 0.3 GeV. A photon was rejected if it was consistent with being from π^0 decay, defined as $M_{\gamma\gamma}$ between 0.10 and 0.17 GeV/c^2. All remaining candidates with $Z_{K\pi\gamma} > 0.5$ were accepted.

The mass difference $\Delta M \equiv M_{K^-\pi^+\gamma} - M_{K^-\pi^+}$ is shown in Fig. 6. The background is estimated from the side bands of D^0. A Monte Carlo study shows that a photon originating from a π^0 which was not removed by the selection cuts, when combined with a D^0, results in a peak at around 75 MeV/c^2; in fact, a hint of such a peak is observed in the data. After subtracting the background, the resulting signal for $D^{*0} \to D^0\gamma$ is 49 ± 14 events. The error includes the uncertainty in the background. In order to determine the D^{*0} fragmentation function, the above analysis was repeated for four Z regions. The fragmentation function is compared in Fig. 7 with that for the D^{*+} [8] and with the JADE D^{*0} data.[9] The curve is a fit of the Peterson fragmentation function to the D^{*+} data. The D^{*0} results are consistent with that for D^{*+}.

A similar analysis was performed for the decay mode $D^{*0} \to D^0\pi^0$. Since the detection efficiency for this mode is small in our detector, only a few candidates were found. After background subtraction, the signal is 16 ± 11 events. Assuming that the only decay modes of the D^{*0} are $D^0\gamma$ and $D^0\pi^0$, the resulting branching ratio for $D^{*0} \to D^0\gamma$ is 0.47 ± 0.23, where the error includes the statistical error and uncertainties in acceptance calculations. This value is independent of the $D^0 \to K\pi$ branching ratio, since it is common to both $D^0\gamma$ and $D^0\pi^0$ decays.

3. Scalar and Tensor Mesons

I will quickly show the results related to a light quark spectroscopy because I am in a heavy quark session. According to the physical picture of string fragmentation model, the spin of a particle comes from an orbital angular momentum: $s = \ell = |\vec{r} \times \vec{p}|$. If I use a typical size of a hadron (r = 1 fm), a mean P_T of a string (p = 300 MeV), and a well-known relation of 1 fm = $\hbar c$/200 MeV/c, then I get $s = (1 \sim 2)\ \hbar$. Therefore, the tensor mesons are expected but the scalar mesons in a high mass region are difficult to incorporate in the string model. It has been suggested that the scalar mesons such as $f_0(975)$ and $a_0(980)$ could be the bound states of $K\bar{K}$, thus four-quark states ($qq\bar{q}\bar{q}$).[10]

We report the production of $f_0(985)$, $f_2(1270)$, and $K_2^*(1430)$.[11] The production cross sections are summarized in Table 1. The fragmentation function of the tensor mesons are in good agreement with the predictions of

the Webber cluster model as shown in Fig. 8.

4. Strange Baryons

We briefly report on the production of strange baryons $\Sigma(1385)^{\pm}$ and Ξ^-.[12] Those particles were observed through their $\Lambda\pi$ decay mode, where the Λ was identified by its weak $p\pi^-$ decay. The details of the selection criteria are skipped here. Figure 9 shows a clear enhancement for $\Sigma(1385)$ in the $\Lambda\pi$ invariant mass plot. The search for Ξ^- production was also performed by selecting its long-lived $\Lambda\pi^-$ decay mode. Table 2 summarizes our results as well as the data from other experiments[13] and the predictions of models. The results are in good agreement with the Lund string model, but they disagree with the Webber cluster model.

5. Charm Baryons

Finally, we show the preliminary analyses on the production of charm baryons $\Lambda_c(2280)$ and $\Sigma_c(2450)$. We attempted to reconstruct Λ_c through its $pK^-\pi^+$ decay mode. Since we do not use the particle identification, there is large combinatorial background as shown in Fig. 10. There is no clear signal. However, if we use the $\Lambda_c \to \bar{K}^0 p$ decay mode, there is an enhancement in the invariant mass distribution at $m = 2.17$ GeV/c^2 with $\Gamma = 200$ MeV/c^2. According to a Monte Carlo simulation, the peak is not a reflection of $D^+ \to \bar{K}^0\pi^+$. The background tends to increase in the upper half of the mass plot. There is also a hint of signal in the decay mode $\Lambda_c \to \Lambda^0\pi^+$.

Another interesting attempt is to look at the decay modes $\Sigma_c^0 \to \Lambda_c^+\pi^-$ and $\Sigma_c^{++} \to \Lambda_c^+\pi^+$. The Σ_c^0 consists of the (ddc) quarks and the Σ_c^{++} of the (uuc) quarks. Therefore, we expect different masses for these particles on the analogy of $M_{\Sigma^-} - M_{\Sigma^+} = 8$ MeV/c^2. However, there are suggestions based on QCD potentials and other mechanisms that the masses are almost same for the Σ_c^0 and Σ_c^{++}. The most accurate measurement on the $\Sigma_c^{++} - \Lambda_c^+$ mass difference is (166 ± 1) MeV/c^2.[14] The low Q-value for the reaction $\Sigma_c \to \Lambda_c\pi$ indicates that the mass difference method should work if the Λ_c comes mainly from the Σ_c production like the case for D and D^*. Figure 11 shows the mass difference $\Delta \equiv M_{pK^-\pi^+\pi^{\pm}} - M_{pK^-\pi^+}$. There is no enhancement around 166 MeV/c^2 so far. This, in turn, puts a preliminary upper limit on the production cross section of Σ_c to be 20% of that for Λ_c.

6. Conclusions

We have reported the HRS results on the production of various hadrons; scalar, tensor, and charm mesons ($f_0(975)$, $f_2(1270)$, $K_2^*(1430)$, $D^*(2007)^0$, and $D^*(2010)^+$), and strange and charm baryons (Ξ^-, $\Sigma(1385)^{\pm}$, Λ_c, and Σ_c). Because

of its clear environment, e^+e^- annihilation is a nice place to look at various resonances (old and new ones).

There are two models that have been tuned well and give us insight into the production mechanisms of hadrons. One is the cluster fragmentation model and the other is the string fragmentation model. However, the mechanism of baryon production has not been understood well, yet. Since these models are also important in the higher energy region, we need even finer tuning and better understanding.

Finally, e^+e^- annihilation is also a nice place to look for exotic resonances such as four-quark states ($qq\bar{q}\bar{q}$), glueballs (gg), and hybrid resonances ($q\bar{q}g$), if the statistics allows.

REFERENCES

1. D. Bender et al., Phys. Rev. D30, 515 (1984).
2. E. Eichten, K. Gottfried, T. Kinoshita, K. D. Lane, and T. M. Yan, Phys. Rev. D21, 203 (1980).
3. Review of Particle Properties, Particle Data Group, Phys. Lett. 170B (1986).
4. R. L. Thews and A. N. Kamal, Phys. Rev. D32, 810 (1985); H. Hallock, S. Oneda, and M. Slaughter, Phys. Rev. D15, 884 (1977).
5. See the summary talk by J. L. Rosner at this conference. Some people expect $B_r(D^{*+} \to D^+\gamma) < 5\%$.
6. K. Jagannathan, A. Jawahery, R. Namjoshi, and C. G. Trahern, Phys. Rev. D32, 1935 (1986).
7. E. H. Low et al., Phys. Lett. 183B, 232 (1987).
8. M. Derrick et al., Phys. Lett. 146B, 261 (1984).
9. W. Bartel et al., Phys. Lett. 161B, 197 (1985).
10. R. L. Jaffe, Phys. Rev. D15, 267 (1977); H. J. Likpin, private communication.
11. S. Abachi et al., Phys. Rev. Lett. 57, 1990 (1986).
12. S. Abachi et al., ANL-HEP-PR-87-26 (to be published in Phys. Rev. Lett.).
13. S. R. Klein et al., Phys. Rev. Lett. 58, 644 (1987); M. Althoff et al., Phys. Lett. 130B, 340 (1983), Z. Phys. C26, 181 (1984).
14. P. C. Bosetti et al., Phys. Lett. 109B, 234 (1982).

ARGONNE-INDIANA-MICHIGAN-PURDUE-SLAC-LBL

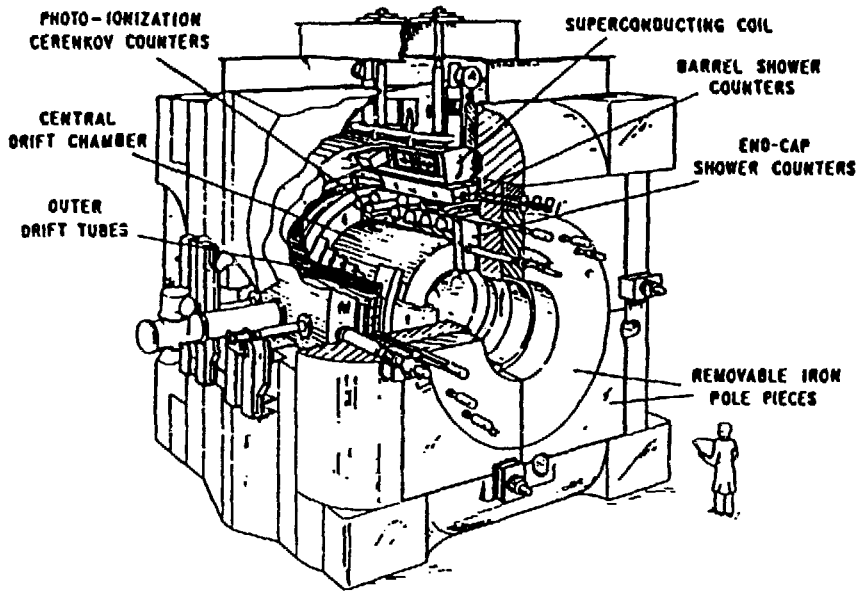

HIGH RESOLUTION SPECTROMETER

Figure 1

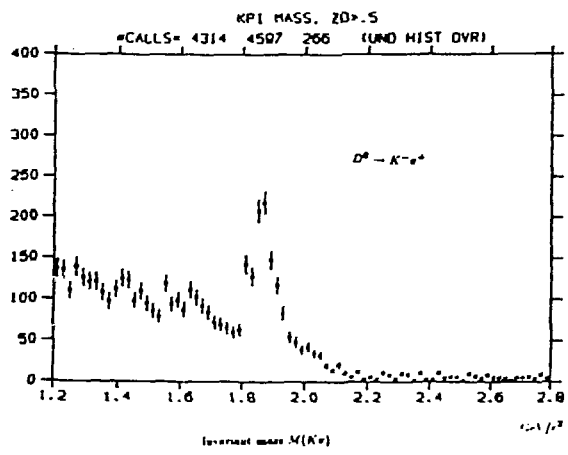

Figure 2

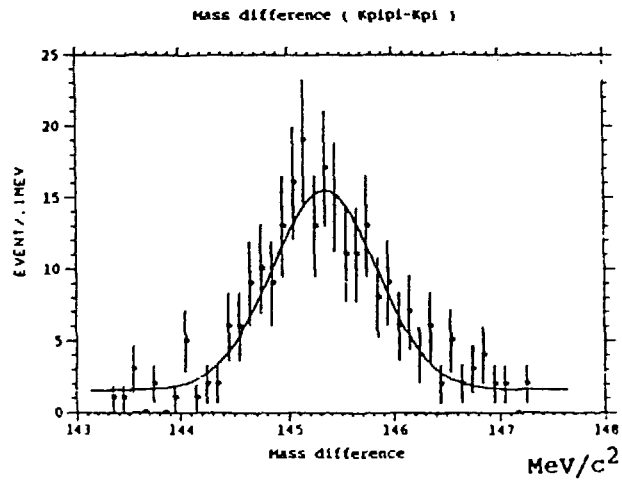

Figure 3

x	$\frac{s}{\beta}\frac{d\sigma}{dz}$ $(nb.GeV^2)$		
	f^0	S	$K^{*0}(1430)$
0.15	140±67	80±35	230±180
0.25	110±60	50±30	80±65
0.35	32±12	31±25	60±45
0.55	23±9	.	8±5

Table 1. Differential cross sections $s/\beta\ d\sigma/dz$ ($z = E/E_{beam}$) for f^0, S, and $K^*(1430)$ mesons for various x intervals ($x = p/p_{beam}$).

	Experiment †				Model	
	TPC	TASSO	MARK II	This Experiment	Lund	Webber
$\Sigma^{\pm}(1385)$/event	0.06±0.03	< 0.09		0.033±0.008	0.032	0.113
$\Sigma^{\pm}(1385)$/A	0.32±0.16	< 0.3		0.15±0.04	0.16	0.35
Ξ^-/event	0.020±0.009	0.026±0.012	0.017±0.006	0.016±0.006	0.017	0.037
Ξ^-/A	0.101±0.046	0.087±0.042	0.08±0.03	0.073±0.028	0.08	0.115

† When both given, the statistical and systematic errors are added in quadrature.

Table 2. The $\Sigma^{\pm}(1385)$ and Ξ^- production rates measured by different collaborations in high energy e^+e^- annihilations, and the comparison with models.

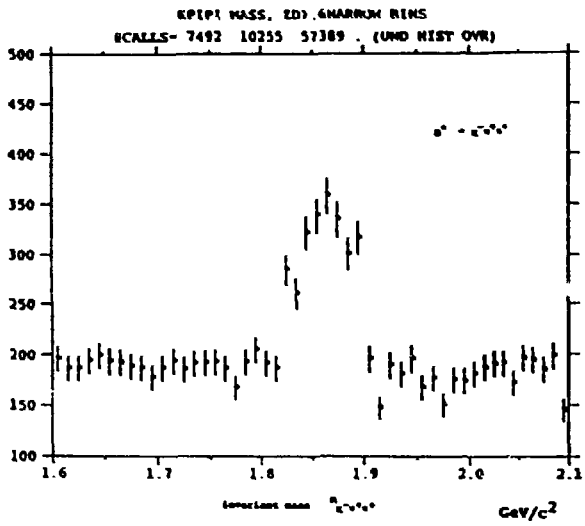

Figure 4

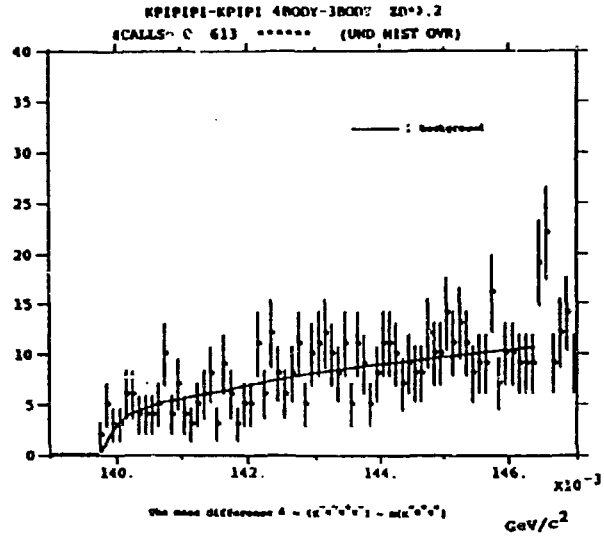

Figure 5

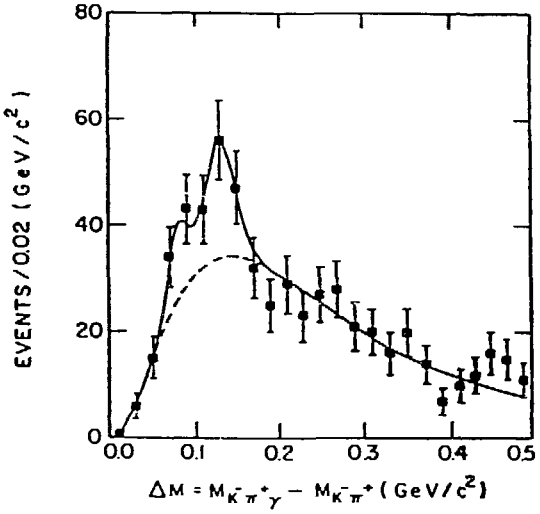

Figure 6

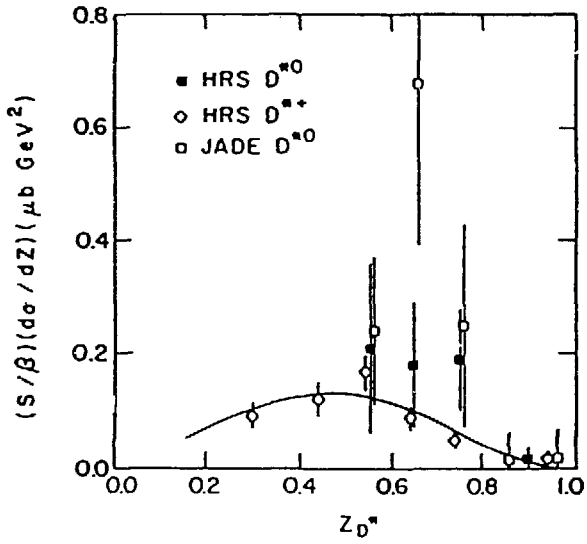

Figure 7

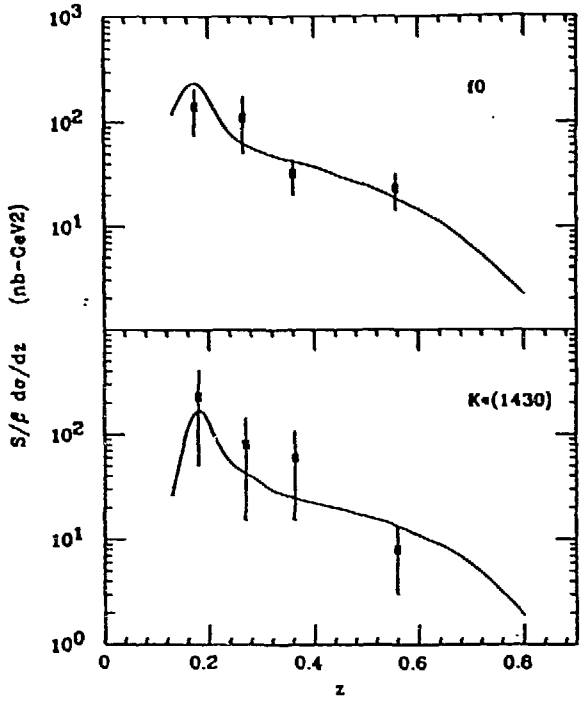

Figure 8

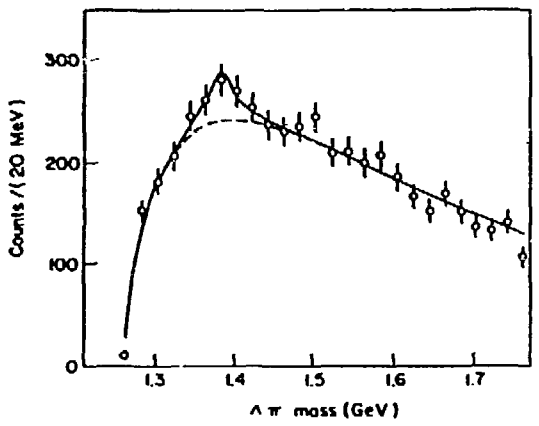

Figure 9

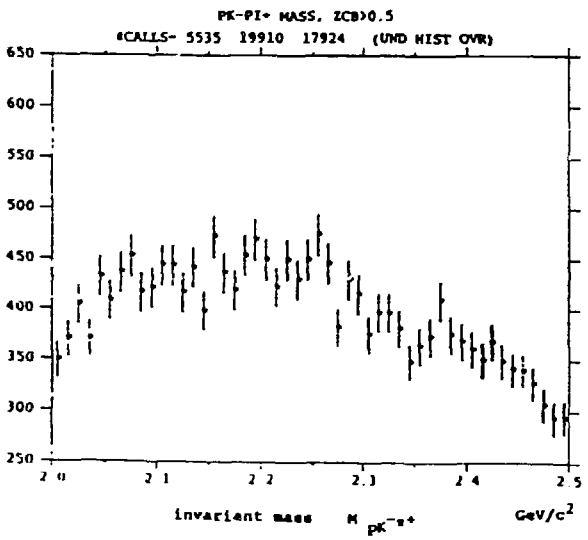

Figure 10

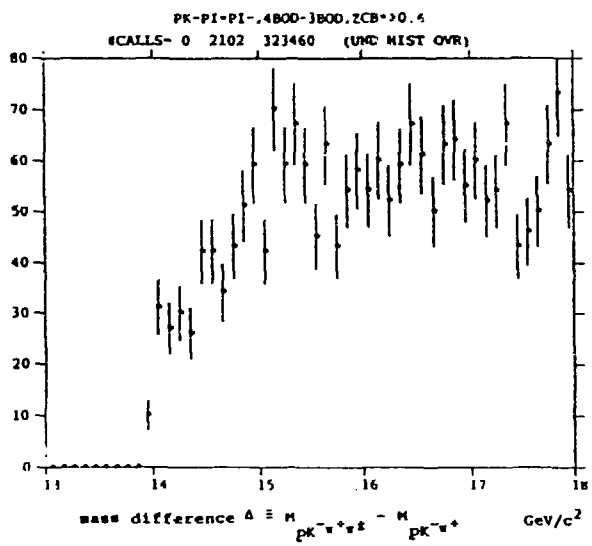

Figure 11